PHYSICAL REVIEW B VOLUME 24, NUMBER 10 15 NOVEMBER 1981

Magnetoconductance study of accumulation layers on *n*-InAs

H. Reisinger, H. Schaber,* and R. E. Doezema†
Physik-Department, Technische Universität München, D-8046 Garching, Federal Republic of Germany
(Received 19 February 1981)

Far-infrared cyclotron resonance and Shubnikov–de Haas oscillations are used to explore accumulation-layer properties of degenerate *n*-InAs. The bulk concentrations studied range from 2×10^{15} to 1×10^{17} cm^{-3}. At the lowest concentration, subband masses, occupations, and relaxation rates are found which are in general agreement with earlier work. For the higher concentrations, the Shubnikov–de Haas oscillations exhibit effects characteristic of a degenerate semiconductor as predicted by Baraff and Appelbaum: Abrupt changes in bound carrier density occur when an additional subband is populated and are compensated by a corresponding decrease of mobile charge at the surface. The self-consistent accumulation potential supports more bound states than observed in earlier tunneling work. A determination of the binding energies of these states results from our measurement of subband masses and occupations.

I. INTRODUCTION

Accumulation layers on *n*-InAs have been the object of a number of recent studies. Tsui[1,2] was the first to explore the structure of subband ladders in the accumulation potential. He exploited a tunneling technique to observe the combined effects of electric and Landau quantization in a naturally existing accumulation layer. In general, however, it is not possible to significantly vary the electric binding potential in such tunneling experiments. In a variable accumulation layer on InAs, the subband structure was characterized in Shubnikov–de Haas (SdH) studies.[3–5] These investigations were performed on low-concentration, epitaxial films. The bulk carrier concentrations in these films were about an order of magnitude lower than the concentration range studied by Tsui (10^{16} cm^{-3} $< n < 10^{18}$ cm^{-3}).

Considerable interest attaches to the InAs results, because InAs is a degenerate semiconductor. In contrast to the case of inversion on such semiconductors [e.g., PbTe (Ref. 6)], the subband structure in accumulation is expected to reflect the influence of "free" bulk carriers which aid in screening the static electric field normal to the interface (Fig. 1). The theoretical work of Baraff and Appelbaum[7] has addressed the problem of bound and mobile-carrier systems coupled through the self-consistent electrostatic potential.

In this paper we present the results of an experimental study of accumulation layers on *n*-InAs. Both cyclotron resonance and SdH oscillations on the same samples are used to yield cyclotron masses, subband occupations, and relaxation rates. Our experiments are performed on low-concentration, epitaxial samples as well as on bulk samples with concentrations in the range studied by Tsui. Our goal is to obtain a consistent experimental description of the InAs accumulation layers and to discuss the results in the context of the Baraff-Appelbaum theory.

Presentation and analysis of our results (Sec. III) follow a brief description of experimental techniques (II). Section IV concludes the paper with a discussion of the results.

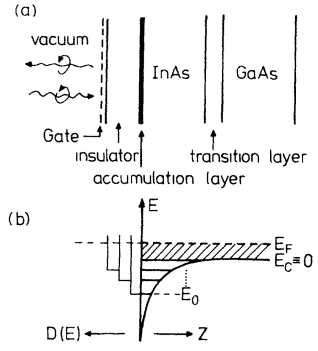

FIG. 1. (a) Sample arrangement. The "transition" and GaAs layers apply only to the epitaxial samples. (b) Schematic accumulation potential and two-dimensional density of states.

II. EXPERIMENTAL NOTES

Accumulation-layer cyclotron resonances was observed in the far-infrared reflectivity of our samples. The measurements were performed in the Faraday geometry, i.e., with the magnetic field $\vec{H}$ normal to the sample plane, along the incident wave vector. The reflectivity contained contributions from the various component layers comprising the samples (Fig. 1). To reduce the interpretational difficulties of unavoidable interference structure, it was advantageous to use circularly polarized radiation. Before reflection off the sample, the far-infrared radiation, produced by a gas laser, was polarized in a circular polarizer unit located within our superconducting magnet (see Fig. 2). The circular polarizer is described in detail in Ref. 8. To enhance the accumulation-layer reflectivity, we measured the accumulation-layer reflectivity, $\Delta R = R(V_G,H) - R(V_{FB},H)$, by square-wave modulating the gate voltage between the value V_G and the flatband voltage V_{FB} while sweeping the magnetic field H.

The gate voltage was applied across a conventional MIS (metal-insulator-semiconductor) sandwich. Two sample types were used. The first is the epitaxial type described by Wagner, Kennedy, and Wieder.[3] The second type of sample consisted of highly polished, plane-parallel slabs of thickness ~ 0.1 mm, with (111) orientation.[9] A layer of SiO_2 (~ 1000 Å) was deposited onto the InAs surfaces. The gate was a semitransparent metal layer evaporated onto the SiO_2. For conductivity measurements, indium contacts to the InAs were used.

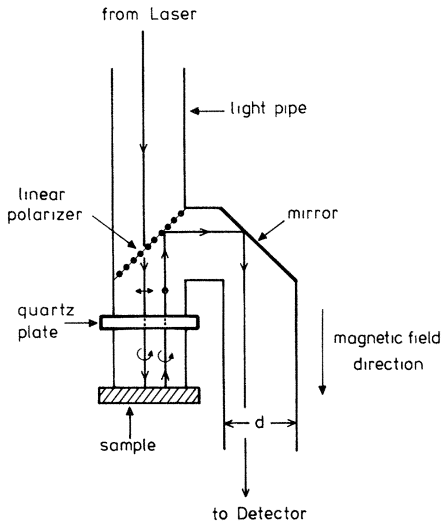

FIG. 2. Circular polarizer unit.

III. RESULTS AND ANALYSIS

Four bulk concentrations were studied: 2×10^{15}, 2×10^{16}, 5×10^{16}, and 1×10^{17} cm^{-3}. In the lowest concentration, epitaxial samples, the bulk carriers play a nearly negligible role. We, therefore, first examine this "nondegenerate" limit.

A. Nondegenerate limit

1. *Measurements and fitting procedure*

Our SdH results were in close agreement with the measurements of Wagner, Kennedy, and Wieder[3] on the epitaxial samples. From these data we identified the flatband voltage as the threshold voltage of the lowest subband.

A set of ΔR traces for various values of V_G at the laser frequency $\hbar\omega = 15.8$ meV is shown in Fig. 3. The gate voltages have been converted to the total concentration values N_s according to $N_s = (1.91\pm0.06)\times10^{11}\,(V_G - V_{FB})$ cm^{-2} for the sample of Fig. 3, where V_G and V_{FB} are in volts. (This relation was calculated from the measured device capacitance at 20 K and the gate area.) The sample temperature was held at 20 K to avoid modulation of the curves, present at lower temperatures, due to quantum oscillations. Such oscillations,[10] characteristic of the completely quantized

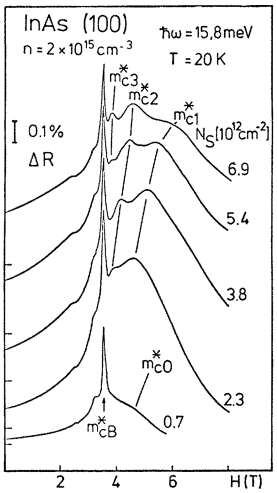

FIG. 3. Differential reflectivity as a function of magnetic field for fixed accumulation densities in the cyclotron resonance active mode. The zero of each trace is indicated.

electron gas, occur when Landau levels pass through the Fermi level as the magnetic field is swept through the cyclotron resonance line.[11]

Some qualitative comments concerning the general features of the curves of Fig. 3 are in order. First, the very sharp structure marked m^*_{cB} occurs at the field value expected for bulk cyclotron resonance[12,13] and is associated with the structure in the sample reflectivity which exists at nonaccumulation gate voltages. Its position does not vary with gate voltage. The broad structure upon which the sharp structure is superimposed is the surface cyclotron resonance[10] of accumulation-layer electrons. With increasing gate voltage (i.e., with increasing N_s), distinct peaks become apparent which shift to higher magnetic fields. These are characteristic of multisubband cyclotron resonance in a semiconductor where nonparabolicity causes an increasing effective mass as each subband edge is lowered from the Fermi energy.[14]

To analyze the data quantitatively, we use a simple oscillator model to fit the differential reflectivity of the MIS sandwich, as was done for PbTe.[6] A representative fit is shown in Fig. 4, where the flat-band reflectivity $R(H)$ is shown together with the contribution of each subband to the total $\Delta R(H)$. The most important parameters are the cyclotron mass m^*_{ci}, the relaxation time τ_i, and the electron concentration N_{si} for each subband i. Before discussing the values we obtain for these parameters, we relate details concerning the ingredients of the $\Delta R(H)$ calculation.

The gate electrode had a resistance of about 50 Ω per square (measured at room temperature). Therefore it was necessary to include its contribution into the calculation of the sample reflectivity in order to obtain $R(H)$ curves as in Fig. 4, which agree both in shape and magnitude with the experimental results. The gate dielectric, however, could be neglected, because its thickness was always less than 1% of the far-infrared wavelength. Also, a low-mobility transition layer (Fig. 1) exerts an important influence on the shape of the calculated curves. This is a layer of $Ga_{1-x}In_xAs$ with x varying from 0 to 1 to accommodate the transition from the semi-insulating GaAs substrate to the InAs epilayer.[5] Its principal effect is to absorb sufficient far-infrared intensity to render reflections from the GaAs negligible (thus making a reflectivity measurement preferable to a transmission measurement where the GaAs substrate and associated interference structure would contribute decisively to the results). To simulate the effect of the layer, we assumed a 1-μm thick layer with magnetic-field-independent refractive indices. These were estimated assuming a carrier concentration of 2×10^{17} cm^{-3} and a frequency–relaxation-time product $\omega\tau=0.5$.

We thus end up with a four-layer interference problem consisting of vacuum, InAs, transition layer, and GaAs substrate. The contribution of the accumulation layer and also the gate electrode is taken into account in the usual way,[15] by modifying the complex reflection amplitude between layer 1 (vacuum) and layer 2 (InAs) according to

$$\hat{r}_{12}=\frac{1-\hat{n}_2+\frac{i\omega}{c}\hat{\epsilon}_{2d}}{1+\hat{n}_2-\frac{i\omega}{c}\hat{\epsilon}_{2d}} . \tag{1}$$

$\hat{n}_2$, the complex refractive index of the InAs layer, is determined by the bulk carrier density n, conduction-band-edge mass m^*_{CBE}, and bulk relaxation time τ. The conductivity $\sigma_{2d}(N_s,H)=i\omega/4\pi\epsilon_{2d}(N_s,H)$ in cgs units and for the cyclotron-resonance-active (CRA) mode is given by

$$\sigma_{2d}(N_s,H)=3.86\times10^{10}\frac{\mathrm{cm}}{\mathrm{sec}}+\sum\frac{N_{si}e^2}{\omega m^*_{ci}}\left[\frac{1}{\omega\tau_i}-i\left[1-\frac{eH}{m^*_{ci}\omega}\right]\right]^{-1}+\frac{\Delta N_B e^2}{\omega m^*_{cB}}\left[\frac{1}{\omega\tau_B}-i\left[1-\frac{eH}{m^*_{cB}\omega}\right]\right]^{-1} . \tag{2}$$

The first two terms represent the contributions of gate electrode and bound-state electrons, respectively. The last term is proportional to ΔN_B, the net change per unit area of the number of bulk electrons as a function of gate voltage. It reflects the response of the bulk, degenerate electron gas in screening the external field,[7] and is thus of special interest.

From fitting the magnetoreflectance at 118, 84, and 78 μm, and taking nonparabolicity into account, we find $m^*_{\mathrm{CBE}}=(0.0246\pm0.0005)m_e$. This is in agreement with the value given by Pidgeon, Mitchell, and Brown,[12] but is somewhat higher than the result of Litton, Dennis, and Smith.[13] The nominal concentration, $n=2\times10^{15}$ cm^{-3}, of our sample was consistent with our data at 20 K,

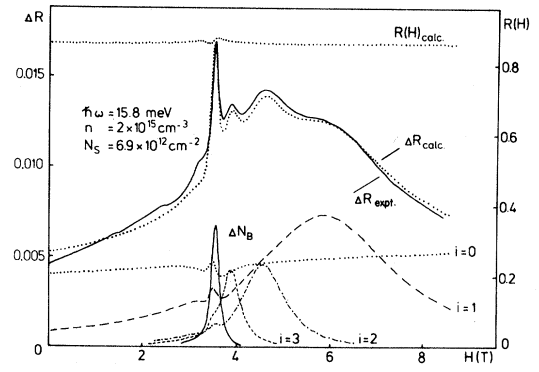

FIG. 4. Fit of the differential reflectivity. Also included is the total sample reflectivity at flatband and the separate contributions to ΔR from each subband i and from the bulk screening charge ΔN_B.

and was therefore the value adopted in the fits. The value for ΔN_B used for Fig. 4 was 1.2×10^{11} cm^{-2}. However, we believe this to be artificial, since the ΔR peak which gives rise to this value (see Fig. 4) contains a "masking" contribution. Such a "masking" arises whenever an additional reflective layer (in this case the accumulation layer) is placed between source and medium (the bulk layer). Even if the conductivity of the accumulation layer is independent of H, every structure $R(H)$ appears also (with negative sign) in $\Delta R(H)$, because the reflectivity change effected by the accumulation layer depends on the absolute magnitude of $R(H)$ already present (see, e.g., the structure at $H\approx3.5$ T in the $i=0$ curve of Fig. 4). In addition, changes in total number of bulk carriers lead to a shift in dielectric anomaly position and thus to a distortion of line shapes in this narrow region of magnetic field. Although these effects are automatically included in the calculation, fitting errors are too large at this point to clearly separate out the contribution of ΔN_B and the value quoted above for Fig. 4 is to be taken as an upper bound. A final bulk parameter which enters the fitting is the scattering rate. At 118 μm we found $\omega\tau=30$ to satisfactorily describe the data; it was also in reasonable agreement with the sample mobility.

2. *Subband parameters*

Having described the bulk parameters and their values chosen for the fit, we now turn to the primary objects of interest, the values for the subband parameters, N_{si}, m_{ci}^*, and τ_i.

In general, values for subband occupation N_{si} are given more accurately by analysis of SdH data than by cyclotron resonance. The SdH values are consistent with our magneto-optical data and were, therefore, adopted. We found $N_{s0}=(1.41\pm0.06)\times10^{11}$ (V_G-V_{T0}) cm^{-2}, $N_{s1}=(0.39\pm0.02)\times10^{11}$ (V_G-V_{T1}) cm^{-2}, and $N_{s2}=(0.12\pm0.01)\times10^{11}$ (V_G-V_{T2}) cm^{-2}, where the gate voltages at which the subbands become occupied are $V_{T0}=V_{FB}=-11.6\pm0.5$ V, $V_{T1}=-11.3\pm0.5$ V, and $V_{T2}-7.5\pm1.0$ V. These results are in good agreement with those quoted by Wagner *et al.*[3] The highest subband, $i=3$, observed in our experiment is hinted at in the SdH data.[3] As seen in Fig. 3, its existence is immediately apparent in cyclotron resonance. For this subband we have taken the N_{s3} values from fitting the magneto-optical data at the various values of V_G. We find $N_{s3}=(0.13\pm0.04)\times10^{11}$ (V_G-V_{T3}) cm^{-2} with $V_{T3}=10\pm4$ V. In such fitting it is the integrated amplitude of each resonance which determines the corresponding N_{si} value.

It is chiefly the positions of the resonance peaks which determine m_{ci}^*. We take the fit values we obtain for the m_{ci}^* at various gate voltages and plot them against the corresponding subband occupations N_{si} as determined above. The results for 78 μm and 20 K are shown in Fig. 5. The resonance from the 0th subband could be clearly identified only at gate voltages just above flatband; only two such points are plotted in the figure. The indicated uncertainties arise mainly from our estimated error in fitting and in the values of N_{si}.

Figure 6 shows the results for the scattering

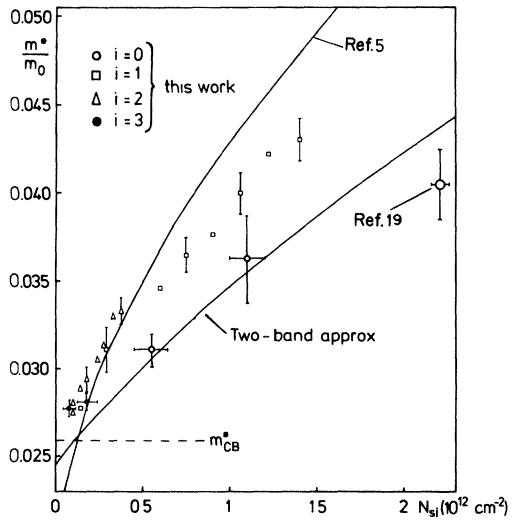

FIG. 5. Subband cyclotron masses as a function of subband occupation from fitting to the data of Fig. 3.

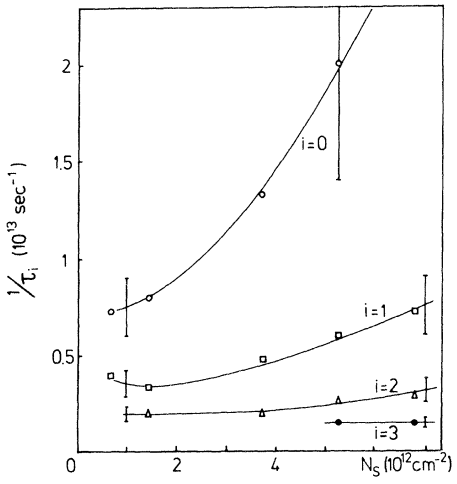

FIG. 6. Subband scattering rates obtained from the data of Fig. 3.

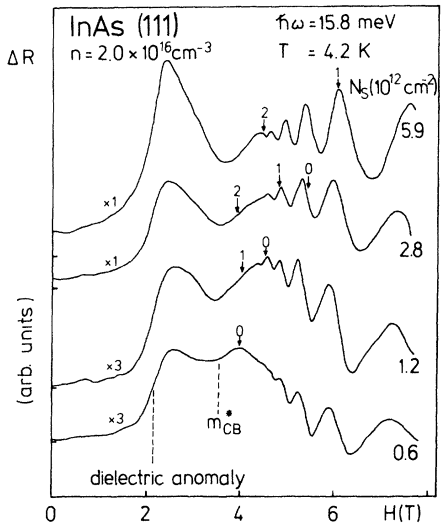

FIG. 7. Differential reflectivity in a 2×10^{16}-cm^{-3} sample in the cyclotron-resonance-active mode; bulk resonance position and dielectric anomaly are indicated. Arrows mark resonance positions for the various subbands as calculated from the measured N_{si} and $m^*_{ci}(N_{si})$ taken from Fig. 5.

rates $1/\tau_i$. Qualitatively the behavior is as expected: The more tightly an electron is bound to the surface, the higher is its scattering rate, reflecting the predominance of surface scattering. The most weakly bound third subband has the lowest rate, which is only about a factor of 3 higher than the bulk rate. At the highest gate voltage, on the other hand, the 0th subband has an extrapolated rate $\sim$25 times higher. Similar values of $1/\tau_i$ are estimated from the SdH oscillations. Taking $\omega_c\tau=1$ at the lowest magnetic field where the oscillations are observable we obtain: $1/\tau_0\approx2\times10^{13}$ sec^{-1}, $1/\tau_1\approx1\times10^{13}$ sec^{-1}, $1/\tau_2\approx0.5\times10^{13}$ sec^{-1}, and $1/\tau_3\approx0.3\times10^{13}$ sec^{-1}.

B. Degenerate case

1. Measurements

In the samples with bulk concentrations 2×10^{16}, 5×10^{16}, and 1×10^{17} cm^{-3} it was considerably more difficult to extract useful fit parameters from our magneto-optical data. The immediate reason for this difficulty is apparent in Fig. 7, where representative traces of the magnetoreflectivity are shown for a 2×10^{16}-cm^{-3} sample. Owing to an increase in $1/\tau_i$ over the 2×10^{15}-cm^{-3} sample, instead of resolved cyclotron resonance peaks, in general, only a broad maximum is seen. Furthermore, above the bulk cyclotron resonance, the helicon modes in our plane-parallel slabs are modified by the space-charge layer thus causing oscillations in ΔR.[16] These oscillations obscure the bound-electron resonances and further hamper the fitting.

The magnetoreflectance curves observed for the high-concentration samples are consistent, however, with the mass values shown in Fig. 5 for the 2×10^{15}-cm^{-3} sample (see Fig. 7). We turn, therefore, to the surface SdH oscillations as a more promising source of information.

With increasing degree of degeneracy, the conductance contribution of the bound carriers decreases relative to that of the mobile carriers. At $n=2\times10^{16}$ cm^{-3}, for example, the bound-carrier conductance is only about 1% of the total conductance measured between source and drain contacts at the highest accumulation densities. In the modulated transconductance, however, the bulk contribution is suppressed. Thus, even in the highest concentration samples, measurement of SdH oscillations in the bound-carrier magnetoconductance is easily accomplished conventionally.

2. Results

Typical SdH oscillations, characteristic of bound-carrier states, are shown for an $n=1\times10^{17}$-cm^{-3} sample in Fig. 8. Three separate sets of oscillations are seen; each is identified with the Landau levels corresponding to a given subband. At constant gate voltage the observed periodicity in $1/H$ allows one to determine the concentration contribution N_{si} of each subband i. These extract-

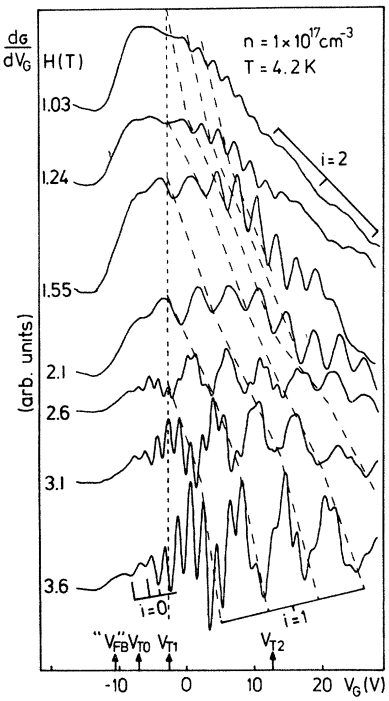

FIG. 8. SdH oscillations in the transconductance as a function of V_G at various magnetic fields in our most degenerate sample. The threshold voltages for each subband are indicated on the V_G axis.

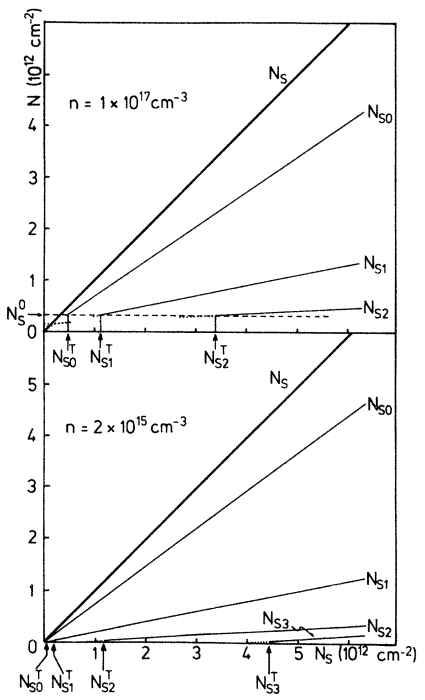

FIG. 9. Subband occupations as a function of total induced carrier density for the most and least degenerate samples. The subband population at threshold, $N_s^0 = 0.24\times10^{11}$ cm^{-2}, for the $n = 2\times10^{15}$-cm^{-3} sample is barely resolved.

ed densities may then be plotted against gate voltage, or against $N_s = (1.35\pm0.02)\times10^{11}(V_G - V_{FB})$ cm^{-2} (determined from the capacitance) as shown in Fig. 9.

It is immediately apparent from this figure that the usual practice of obtaining subband thresholds N_{si}^T, i.e., the value of N_s at which the subband i becomes occupied, by extrapolating the subband densities N_{si} to zero is invalid. This would lead to the contradiction of excited subbands becoming bound before the ground state. The bulk degeneracy of our samples must be invoked to properly interpret our results.

The schematic energy structure for an accumulation layer on a degenerate n-type semiconductor has been indicated in Fig. 1. Each subband becomes bound at the conduction-band edge E_c. The Fermi level E_F lies in the conduction band, however; thus the concentration of a subband at binding must jump discontinuously from zero to the value $N_s^0 = m^*(E)/\pi\hbar^2\ (E_F - E_c)$, using the usual expression for the two-dimensional density of states. Assuming bulk nonparabolicity and band-edge mass for such a weakly bound subband, this value depends only on the bulk concentration n (and not on subband index) and is given by $N_s^0 = \frac{1}{2}(9\pi n^2)^{1/3}$. The coincidence of N_s^0, thus determined, with the N_{si} (N_s) line from the SdH analysis determines the values N_{si}^T (see Fig. 9). Even for the very low concentration, 2×10^{15} cm^{-3}, the degeneracy has a small effect as indicated in the figure. The numerical results for all concentrations studied are contained in Table I. As is to be expected from the picture outlined here, SdH oscillations belonging to a given subband are only observed at and above the gate voltage correspondingly to its value of N_{si}^T. These gate voltages V_{Ti} have been marked in Fig. 8.

Figure 10 gives a more detailed picture at gate voltages near V_{T1} (H sweep). Oscillations due to subband 1 are rapidly quenched when V_G becomes more negative than -2.5 ± 1 V, the V_{T1} value determined from Fig. 9. At $V_G = -6$ V, oscillations corresponding to subband 1 are no longer observed. (The weak oscillations on the two lower traces of Fig. 10 as well as part of the high-field structure in the other traces are due to subband 0.) The presence of $i = 1$ oscillations slightly below V_{T1} ($V_G = -4$ and -5 V) is related to a deviation of N_{s1} (V_G) from its linear behavior in the vicinity

TABLE I. Subband thresholds N_{si}^T and population rates for the samples investigated.

n (cm^{-3})	E_F (meV)	N_s^0 (10^{11} cm^{-2})	$\Delta N_{si}/\Delta N_s$	N_{si}^T (10^{12} cm^{-2})	i
(2.0 ±0.6)×10^{15}[a]	2.4±0.2	0.24±0.02	0.75 ±0.02	0.032±0.003	0
			0.20 ±0.01	0.17 ±0.02	1
			0.064±0.005	1.16 ±0.1	2
			0.06 ±0.02	4.3 ±0.6	3
(2.0 ±0.2)×10^{16}[b]	10.7±0.5	1.14±0.05	0.65 ±0.02	0.17 ±0.01	0
			0.20 ±0.01	0.51 ±0.03	1
			0.063±0.004	1.53 ±0.1	2
(5.1 ±0.1)×10^{16}[b]	19.4±0.3	2.09±0.03	0.66 ±0.02	0.32 ±0.01	0
			0.205±0.004	0.77 ±0.02	1
			0.057±0.004	2.48 ±0.03	2
(1.00±0.02)×10^{17}[b]	29.9±0.5	3.28±0.05	0.68 ±0.02	0.48 ±0.02	0
			0.197±0.003	1.13 ±0.02	1
			0.051±0.004	3.5 ±0.3	2

[a]R. J. Wagner, T. A. Kennedy, and H. H. Wieder, in *Proceedings of the International Conference on the Electronic Properties of Two-Dimensional Systems, Berchtesgaden, July 1977,* edited by P. J. Stiles and G. Durda (North-Holland, Amsterdam, 1979).
[b]Determined by analysis of bulk SdH oscillations.

of V_{T1}, as is shown in the inset of Fig. 10. The lowest subband density observed, however, corresponds to the calculated N_s^0 within the experimental uncertainty of ±5%. This sort of pinning behavior indicates an influence of the most weakly bound state on the long-range part of the surface potential. Detailed understanding of this phenomenon requires further, both experimental and theoretical, investigations.

Within the resolution of our data (±4×10^{10} carriers/cm^2) we observe no discontinuity in the occupation of already bound subbands, when an additional subband is abruptly populated.

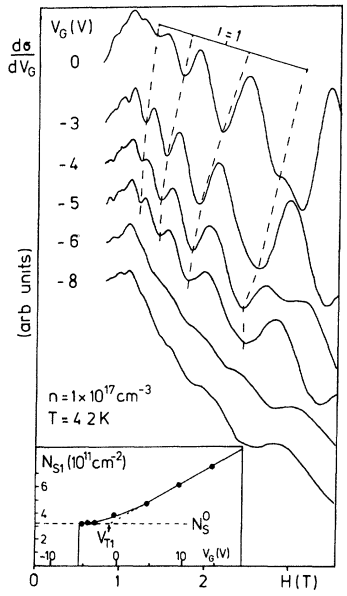

FIG. 10. SdH oscillations as a function of magnetic field at various gate voltages near V_{T1}. Inset shows $N_{s1}(V_G)$ as determined from the observed SdH periods.

IV. DISCUSSION

A. Effective masses

Each subband i of the two-dimensional gas is characterized by its dispersion,

$$E = E_i + \frac{\hbar^2 k_{||}^2}{2m^*} , \tag{3}$$

where E_i is the quantized energy for motion normal to the layer and the parabolic term represents free-electron-like motion in the layer plane. The corresponding density of states (for both spins) is $m^*/\pi\hbar^2$. When the subband edge is at an energy $E_i' \equiv E_F - E_i$ below the Fermi energy, the total number of carriers N_{si} in the subband is $E_i' m^*/\pi\hbar^2$. A measurement of m^* and N_{si}, therefore, allows one to determine E_i'.

In a nonparabolic system the above analysis must be modified. That nonparabolicity is important in InAs is evident from Fig. 5 where the masses are seen to increase as the energies E_i' increase. The values of the E_i are only a fraction of the gap energy [$E_G = 410$ meV (Ref. 12)], however, so that as a first approximation[17,18] one expects the form of the familiar two-band model to describe the mass variation with energy:

$$m^* \cong \left[1+\frac{2E_i'}{E_G}\right] m^*_{\mathrm{CBE}} , \tag{4}$$

where m^*_{CBE} is the mass at the conduction-band-edge. Inserting this expression into the density of states and integrating, we find

$$N_{si} \cong \frac{m^*_{\mathrm{CBE}} E_i'}{\pi\hbar^2}\left[1+\frac{E_i'}{E_G}\right] . \tag{5}$$

Solving this equation for E_i' and inserting the result into Eq. (3), one obtains m^* as a function of N_{si}. This two-band approximation is indicated in Fig. 5. Although it appears to describe the mass variation for the 0th subband, it clearly underestimates the masses of the excited subbands. We expect the subband masses to extrapolate to the observed bulk mass at $N_{si}=0$ rather than to the band-edge mass. This results from nonparabolicity due to the finite frequency, $\hbar\omega = 15.8$ meV, at which the masses are measured.

In Fig. 5 we have also indicated a 0th subband mass value extracted from Tsui's measurement[19] using his correction factor.[2] Tsui's mass, which was determined in an $n = 5.4\times10^{17}$- cm^{-3} sample, appears to be consistent with our values for this subband. Also seen in the figure is the result of a calculation (more sophisticated than our two-band estimate) by Washburn, Sites, and Wieder[5] of the subband mass variation with N_{si}. They also obtained experimental values of the subband cyclotron masses from the temperature dependence of the SdH oscillations. These values lie close to, but slightly above, their calculation. Above about 0.5×10^{12} cm^{-2}, our results and the SdH masses deviate. The reason for this is not clear; we note, however, that large correction factors, $\sim$20%, were used in determining the SdH masses.[5]

B. Subband energies

As mentioned above, one can use the measured effective masses and subband occupation densities to predict the subband energies E_i. Nonparabolicity can be included by utilizing Eqs. (4) and (5). Using the experimental masses measured in the 2×10^{15}-cm^{-3} sample (Fig. 5) and the N_{si} values from Table I, we arrive at the results plotted in Fig. 11. Systematic errors may be introduced here, if the subband masses depend strongly on bulk carrier concentration, or if large deviations from the two-band model assumed in calculating the density of states occur. Both these corrections seem to be small in our case considering the good agreement

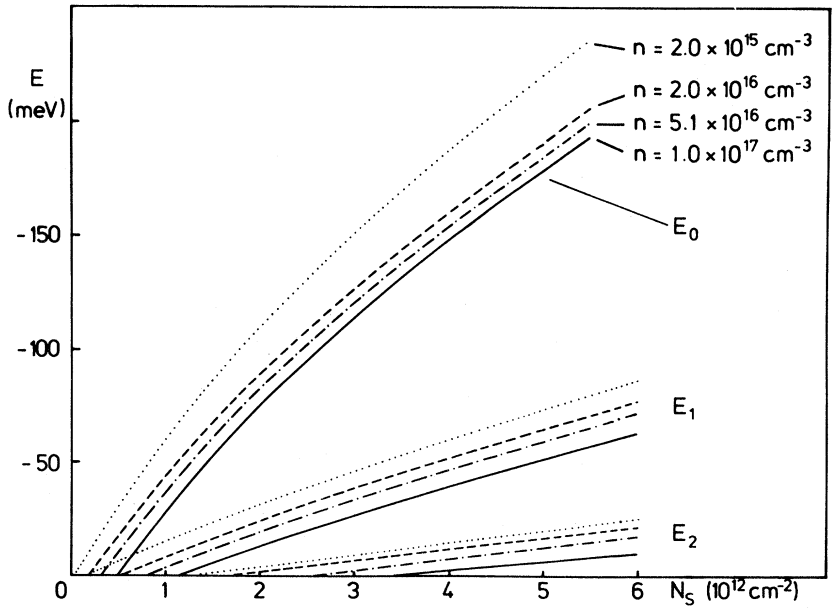

FIG. 11. Subband binding energies measured from the conduction-band edge versus total carrier density.

of our subband cyclotron masses with Tsui's data and the consistency among our different concentration samples. We therefore estimate systematic errors in E_i to be only a small fraction of the total nonparabolicity correction (maximum of 40% for $i=0$); experimental errors in N_{si} and m_{ci}^* lead to an uncertainty in E_i of $\pm 10\%$ or less. From this plot one can read off intersubband energies for transitions from subband edge to subband edge: $\hbar\omega_{ij} = E_i - E_j$ as a function of N_s. This prediction is in reasonable agreement with observed values.[20]

It is also of interest to compare our subband energies E_i to the (zero-bias) binding energies found by Tsui.[2] In a 1.3×10^{17} cm^{-3} sample he finds two bound states with 2×10^{12} and 7.7×10^{11} cm^{-2} surface electron densities. Comparing this result to ours in the 1×10^{17} cm^{-3} sample, we find that when our ground state contains 2×10^{12} cm^{-2} electrons, the first excited state has 7×10^{11} cm^{-2}, and the second excited state is not yet bound (Fig. 9). Thus the numbers are compatible with Tsui's and with his observation of only two bound states in his layer of (quasi) fixed density. In his lowest concentration samples (2.2×10^{16} cm^{-3}), however, Tsui also observes only two bound states. Our Fig. 11 predicts that, for this concentration, three bound states should be observed whenever E_0 exceeds about 80 meV. For Tsui's observation of only two bound states to be consistent with our data, his ground-state bias voltages $\sim$170 meV would need to be severely adjusted to produce a zero bias $E_0 \lesssim 80$ meV. An alternative possibility is that a third bound-state tunneling dip contributes to the structure due to the conduction-band edge in Tsui's data. (The binding energy of the third state would be small, $\sim$10 meV.) This possibility was, however, considered unlikely by Tsui[19] because of the absence of third-state Landau-level oscillations in the tunneling current.

C. Comparison with theory

Up to now we have avoided discussion of the determination of the total induced concentration $N_s(V_G)$. The difficulty does not lie in finding the slope $\Delta N_s/\Delta V_G$: It is uniquely fixed by the measured capacitance. The difficulty lies in determining the gate voltage at which $N_s=0$, i.e., the "flatband" voltage $V_{\rm FB}$. For the N_s axis in Fig. 9, we set $N_s=0$ at the gate voltage where the ground-state density N_{s0} extrapolates to zero. Although this is a reasonable procedure in the low-concentration, nondegenerate limit (2×10^{15} cm^{-3}), it is arbitrary for the higher concentrations.

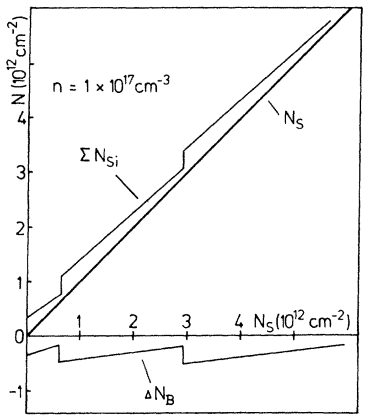

FIG. 12. Comparison of bound-state density and total induced charge with the zero of N_s shifted from that of Fig. 9 to N_{s0}^T.

To determine $V_{\rm FB}$ in the degenerate limit, we turn to the theoretical work of Baraff and Appelbaum.[7] They find that even with no external electric field (i.e., at "flatband") there exists a self-consistent potential well of sufficient strength to support a bound state for values of the bulk effective inter-electron spacing $r_s < 1.0$. In InAs this corresponds to concentrations of $n > 7\times10^{15}$ cm^{-3}. The binding energy is found to be only a few percent of $E_F - E_c$, thus the bound state contains $\sim N_s^0$ electrons, and therefore $V_{\rm FB} \approx V(N_{s0}^T)$. Following this argument, we are justified in taking $N_s=0$ at the threshold voltage $V(N_{s0}^T)$ of the ground-state subband. In Fig. 12 we have replotted the results for $n=1\times10^{17}$ cm^{-3} from Fig. 9, again neglecting pinning effects in the vicinity of the N_{si}^T (cf. Fig. 10). In Fig. 9, one observes no discontinuities in the N_{si} values of lower-lying subbands when a new subband is bound. This is in accordance with the Baraff-Appelbaum prediction that the self-consistent potential varies continuously with external field, as also observed by Tsui.[2] Since the total induced charge also varies continuously with gate voltage, the discontinuous increase in total bound-charge density $\sum_i N_{si}$ which occurs whenever a new state is bound, must be compensated by a corresponding decrease in mobile-charge density ΔN_B. As seen in Fig. 12, choosing $N_s=0$ at $V(N_{s0}^T)$ indicates that there is a depletion of mobile charge at the surface which is most pronounced at those gate voltages where a new surface level is bound. As discussed by Baraff and Appelbaum, these compensating, negative discontinuities in ΔN_B reflect the orthogonality requirement of bound- and mobile-electron wave functions.

ACKNOWLEDGMENTS

We are indebted to H. H. Wieder for providing us with the epitaxial samples, to J. S. Götzlich for aid in depositing the SiO_2 layers on the bulk samples, and to R. J. Wagner for helpful communication. We are grateful to F. Koch for his generous encouragement and advice. This work was supported by the Deutsche Forschungsgemeinschaft (SFB 128).

---

*Present address: Siemens AG, Unternehmensbereich Bauelemente, D-8000 München 80, Federal Republic of Germany.

†Present address: Department of Physics and Astronomy, University of Oklahoma, Norman OK 73019.

[1]D. C. Tsui, Phys. Rev. Lett. 24, 303 (1970).

[2]D. C. Tsui, Phys. Rev. B 8, 2657 (1973).

[3]R. J. Wagner, T. A. Kennedy, and H. H. Wieder, in *Proceedings of the 3rd International Conference on the Physics of Small Gap Semiconductors, Warsaw 1977,* edited by J. Rauluszkiewicz, M. Gorska, and E. Kaczmarek (PWN-Polish Scientific, Warsaw, 1978), p. 427; Surf. Sci. 73, 545 (1978).

[4]H. A. Washburn and J. R. Sites, Surf. Sci. 73, 537 (1978).

[5]H. A. Washburn, J. R. Sites, and H. H. Wieder, J. Appl. Phys. 50, 4872 (1979).

[6]H. Schaber and R. E. Doezema, Phys. Rev. B 20, 5257 (1979).

[7]G. A. Baraff and J. A. Appelbaum, Phys. Rev. B 5, 475 (1972).

[8]H. Schaber and R. E. Doezema, Infrared Phys. 18, 247 (1978).

[9]Obtained from HEK Gesellschaft mit beschränkter Haftung, Lübeck, Federal Republic of Germany.

[10]G. Abstreiter, J. P. Kotthaus, J. F. Koch, and G. Dorda, Phys. Rev. B 14, 2480 (1976).

[11]T. Ando, J. Phys. Soc. Jpn. 38, 989 (1975).

[12]C. R. Pidgeon, D. L. Mitchell, and R. N. Brown, Phys. Rev. 154, 737 (1967).

[13]C. W. Litton, R. B. Dennis, and S. D. Smith, J. Phys. C 2, 2146 (1969).

[14]A. Därr, J. P. Kotthaus, and J. F. Koch, Solid State Commun. 17, 455 (1975).

[15]T. Ando, J. Phys. Soc. Jpn. 38, 989 (1975).

[16]H. Reisinger, Diplom thesis, Technische Universität München, 1978 (unpublished).

[17]G. A. Antcliff, R. T. Bate, and R. A. Reynolds, in *Proceedings of the Conference on the Physics of Semimetals and Narrow-Gap Semiconductors, 1970,* edited by D. L. Cater and R. T. Bate (Pergamon, New York, 1971), p. 487.

[18]F. J. Ohkawa and Y. Uemura, J. Phys. Soc. Jpn. 37, 1325 (1974).

[19]D. C. Tsui, Phys. Rev. B 4, 4438 (1971).

[20]H. Reisinger and F. Koch, Bull. Am. Phys. Soc. 25, 388 (1980); H. Reisinger and F. Koch, Solid State Commun. 37, 429 (1981).